







## ARTICLE

# Cardiac mechanical efficiency is preserved in primary cardiac hypertrophy despite impaired mechanical function

June-Chiew Han<sup>1</sup>, Kenneth Tran<sup>1</sup>, David J. Crossman<sup>2</sup>, Claire L. Curl<sup>4</sup>, Parisa Koutsifeli<sup>2</sup>, Joshua P.H. Neale<sup>2</sup>, Xun Li<sup>2</sup>, Stephen B. Harrap<sup>4</sup>, Andrew J. Taberner<sup>1,3</sup>, Lea M.D. Delbridge<sup>4</sup>, Denis S. Loiselle<sup>1,2</sup>, and Kimberley M. Mellor<sup>1,2</sup>

Increased heart size is a major risk factor for heart failure and premature mortality. Although abnormal heart growth subsequent to hypertension often accompanies disturbances in mechano-energetics and cardiac efficiency, it remains uncertain whether hypertrophy is their primary driver. In this study, we aimed to investigate the direct association between cardiac hypertrophy and cardiac mechano-energetics using isolated left-ventricular trabeculae from a rat model of primary cardiac hypertrophy and its control. We evaluated energy expenditure (heat output) and mechanical performance (force length work production) simultaneously at a range of preloads and afterloads in a microcalorimeter, we determined energy expenditure related to cross-bridge cycling and  $\text{Ca}^{2+}$  cycling (activation heat), and we quantified energy efficiency. Rats with cardiac hypertrophy exhibited increased cardiomyocyte length and width. Their trabeculae showed mechanical impairment, evidenced by lower force production, extent and kinetics of shortening, and work output. Lower force was associated with lower energy expenditure related to  $\text{Ca}^{2+}$  cycling and to cross-bridge cycling. However, despite these changes, both mechanical and cross-bridge energy efficiency were unchanged. Our results show that cardiac hypertrophy is associated with impaired contractile performance and with preservation of energy efficiency. These findings provide direction for future investigations targeting metabolic and  $\text{Ca}^{2+}$  disturbances underlying cardiac mechanical and energetic impairment in primary cardiac hypertrophy.

## Introduction

With the exception of age, cardiac hypertrophy is the strongest independent predictor of cardiovascular morbidity and mortality (Levy et al., 1990; Kannel, 1991). Although pathological cardiac growth can be an adaptive response to meet increased hemodynamic load, accumulating evidence shows that cardiac hypertrophy is linked to maladaptive cellular processes that promote heart failure progression, after adjusting for variation in blood pressure and other comorbidities (Levy et al., 1990).

Heart failure is often linked with a disturbance in cardiac mechano-energetic performance, typically exemplified by reduced contractility and energy efficiency (Ishibashi et al., 1996; Laine et al., 1999; Akinboboye et al., 2004). But an understanding of the mechano-energetic consequences of myocardial hypertrophy in the absence of confounding influences such as hypertension, diabetes, myocardial infarction, ischemia, and valvular diseases is limited. In clinical studies, impaired cardiac performance and mechano-energetic disturbances are common

observations in hypertensive patients with cardiac hypertrophy (Ishibashi et al., 1996; Laine et al., 1999; Akinboboye et al., 2004). But not all hypertensive patients develop myocardial hypertrophy (Tingleff et al., 1996), and indeed, successful anti-hypertensive therapy does not necessarily reverse cardiac hypertrophy (Cruickshank, 1992; Cruickshank et al., 1992). In animal studies, disturbed myocardial energetics have been reported in settings of cardiac hypertrophy of systemic hypertensive origin (Han et al., 2014) and of pulmonary hypertensive origin (Pham et al., 2018). Thus, whether disturbed cardiac mechano-energetics arise from the effects of pathological hypertrophy alone or are due to other comorbidities such as hypertensive afterload is unknown. Insight into the effects of cardiac hypertrophy independent of increased blood pressure is important for understanding the increased heart failure risk associated with pathological cardiomyocyte growth.

We have previously developed a normotensive rat model of primary cardiac hypertrophy, originating from identification of

<sup>1</sup>Auckland Bioengineering Institute, University of Auckland, Auckland, New Zealand; <sup>2</sup>Department of Physiology, University of Auckland, Auckland, New Zealand; <sup>3</sup>Department of Engineering Science, University of Auckland, Auckland, New Zealand; <sup>4</sup>Department of Physiology, University of Melbourne, Melbourne, Australia.

Correspondence to Kimberley M. Mellor: [k.mellor@auckland.ac.nz](mailto:k.mellor@auckland.ac.nz).

© 2021 Han et al. This article is distributed under the terms of an Attribution–Noncommercial–Share Alike–No Mirror Sites license for the first six months after the publication date (see <http://www.rupress.org/terms/>). After six months it is available under a Creative Commons License (Attribution–Noncommercial–Share Alike 4.0 International license, as described at <https://creativecommons.org/licenses/by-nc-sa/4.0/>).

blood pressure-independent genetic loci associated with cardiac hypertrophy in the spontaneously hypertensive rat (SHR; [Innes et al., 1998](#)). Crossbreeding of SHRs with Fischer 344 control rats and phenotypic selection generated a stable inbred line of rats with normotensive cardiac hypertrophy ([Harrap et al., 2002](#)), thus affording a unique opportunity for investigation into primary pathological hypertrophy in the absence of hypertension. The etiology of cellular hypertrophy in this model has developmental origins of premature terminal cardiomyocyte differentiation and excess programmed cell death at birth ([Porrello et al., 2009a, 2009b](#)). Pathological hypertrophic markers are elevated in adult hypertrophic hearts, with increased expression of brain natriuretic peptide, atrial natriuretic peptide, and  $\beta$ -myosin heavy chain ( $\beta$ -MHC), associated with increased cardiomyocyte length and width ([Porrello et al., 2009a](#)). The effect of primary cardiomyocyte hypertrophy on myocardial mechanoenergetics has not been previously investigated.

The central goal of this investigation was to determine the underlying mechano-energetic mechanisms of normotensive pathological cardiac hypertrophy. In this study, we have investigated the mechano-energetic properties of left-ventricular (LV) trabeculae isolated from rats with primary cardiac hypertrophy and their controls. Evaluation of cardiac muscle force and length change twitch profiles was performed with simultaneous measurement of energetics (heat production) in a flow-through work-loop calorimeter ([Taberner et al., 2011; Johnston et al., 2015](#)). We conducted a comprehensive study of trabeculae performance at a range of preloads and afterloads, under both isometric and force-length work-loop contractions (simulating the pressure-volume loops of the heart). The energetic cost of  $\text{Ca}^{2+}$  and cross-bridge cycling was evaluated for determination of mechanical and cross-bridge efficiency.

## Materials and methods

### Ethical approval

Experiments were conducted in accordance with the New Zealand Animal Welfare Act with the approval of the University of Auckland Animal Ethics Committee.

### Experimental animals

A rat model of normotensive cardiac hypertrophy was generated through selection and crossbreeding of Fischer 344 and SHR strain progenitors and has previously been described ([Innes et al., 1998; Harrap et al., 2002; Porrello et al., 2009a](#)). Identification of blood pressure-independent hypertrophic genetic loci in the SHRs led to a selective breeding program to simultaneously derive the normotensive hypertrophic rats and control rats with normal heart size and normal blood pressure, now beyond the 50th generation of inbreeding at the University of Melbourne. Experiments were performed on a sub-strain of these animals at the University of Auckland, using male rats at 12–13 wk of age. All experimental animals were housed under a 12-h light/dark cycle at room temperature with water and standard chow provided ad libitum. One cohort of rats was analyzed for cardiac morphology and molecular analysis in LV tissues, and a second cohort was used for trabecula functional studies.

### Cardiomyocyte dimensions and F-actin area

Rats were anesthetized by isoflurane inhalation (<5% in  $\text{O}_2$ ) before euthanasia by cervical dislocation. Hearts were excised and the ventricular midsection dissected and fixed in 2% paraformaldehyde for 10 min followed by cryoprotection in 30% sucrose before freezing in liquid  $\text{N}_2$ -chilled isopentane. The tissue was sectioned (20  $\mu\text{m}$ ), mounted onto coverslips, and blocked in FX signal enhancer solution (Thermo Fisher Scientific) for 30 min. The sections were stained with wheat germ agglutinin (WGA) Alexa-594 and phalloidin Alexa-680 (Thermo Fisher Scientific) for 2 h, diluted 1:50 in PBS containing 1% BSA and 0.1% NaAzide. Sections were mounted in a solution containing 90% glycerol and 10% PBS and images captured on a Zeiss LSM710 confocal microscope using a 63 $\times$  1.4 NA oil-immersion objective and a pixel spacing of 94 nm. Measurement of cell length and width was performed on the WGA-stained images in a blinded manner using ImageJ. For measurement of the percentage of F-actin area, images of phalloidin-stained sections were enhanced (0.3% saturated pixels), and a Gaussian blur (2-pixel radius) was applied. Images were binarized using standardized thresholding, and the area of phalloidin-stained F-actin was determined and presented as a percentage of the total cellular area. Analysis was automated using a custom ImageJ macro.

### Immunoblotting

LV tissue segments were homogenized in 100 mM Tris-HCl, 5 mM EGTA, and 5 mM EDTA, pH 7.0. Tissue homogenates were prepared in loading buffer (50 mM Tris-HCl, pH 6.8, 2% sodium dodecyl sulfate, 10% glycerol, 0.1% bromophenol blue, and 2.5% 2-mercaptoethanol), and equal amounts of protein were loaded into the SDS-PAGE gel. Sample protein concentrations were determined using a Lowry assay. Immunoblot membranes were probed with a primary antibody for SERCA2a (#A010-20; Badrilla) and an anti-rabbit horseradish peroxidase-conjugated secondary antibody (GE Healthcare). The ECL Prime (Amersham; GE Healthcare) chemiluminescent signal was visualized with a ChemiDoc-XRS Imaging device and band intensity quantified using ImageLab software (Bio-Rad). Equal protein loading was confirmed by Coomassie staining of polyvinylidene difluoride membranes (Coomassie Brilliant Blue R-250; Bio-Rad).

### Quantitative PCR mRNA analysis

RNA was extracted and reverse-transcribed and gene expression evaluated by quantitative PCR as previously described ([Mellor et al., 2014](#)). The primer pairs used were as follows: rat Myh6 ( $\alpha$ -MHC): 5'-CGCCAAGAAAATGCACGATGAGGA-3' (forward) and 5'-CGCTGTTGCTATCCCACAATAAATATG-3' (reverse); rat Myh7 ( $\beta$ -MHC): 5'-CTCAAGCTCCTAAGTAATCTGTT-3' (forward) and 5'-GCAAAGAAAGGCTCATCCTTTC-3' (reverse); and housekeeper gene  $\beta_2$ -microglobulin: 5'-CCGTCGTGCTTGCCATTTCAGA-3' (forward) and 5'-CTCAACTGCTACGTGTCTC-3' (reverse). The comparative  $\Delta\Delta\text{Ct}$  method ([Livak and Schmittgen, 2001](#)) was used to analyze the genes of interest relative to the housekeeper gene and presented as fold-change relative to the control group.

Table 1. **Morphometric characteristics of cardiac hypertrophic and control rats**

	Control	Hypertrophy	P value
Body mass (g)	287 ± 5	255 ± 4 <sup>a</sup>	<0.0001
Tibial length (mm)	36.4 ± 0.3	34.1 ± 0.3 <sup>a</sup>	<0.0001
Heart mass (mg)	943 ± 30	931 ± 40	0.7991
Ventricular mass (mg)	903 ± 26	869 ± 37	0.4546
Heart mass per body mass (mg g <sup>-1</sup> )	3.27 ± 0.1	3.65 ± 0.1 <sup>a</sup>	0.0107
Ventricular mass per body mass (mg g <sup>-1</sup> )	3.13 ± 0.1	3.40 ± 0.1 <sup>a</sup>	0.0391
Heart mass per tibial length (mg mm <sup>-1</sup> )	25.8 ± 0.7	27.3 ± 1.1	0.2746
Ventricular mass per tibial length (mg mm <sup>-1</sup> )	24.7 ± 0.6	25.5 ± 1.1	0.5381

Values presented are mean ± standard error,  $n = 18$  or  $19$  rats/group. Data analyzed by Student's  $t$  test.

<sup>a</sup> $P < 0.05$ .

### Cardiac trabeculae preparation

Rats were anesthetized by isoflurane inhalation (<5% in O<sub>2</sub>) and injected with heparin (1,000 IU kg<sup>-1</sup>) before euthanasia by cervical dislocation. The heart was excised, and the aorta was cannulated for Langendorff perfusion with Tyrode solution (in mmol/liter: 130 NaCl, 6 KCl, 1 MgCl<sub>2</sub>, 0.5 NaH<sub>2</sub>PO<sub>4</sub>, 0.3 CaCl<sub>2</sub>, 10 HEPES, 10 glucose, and 20 2,3-butanedione monoxime, pH, 7.4 as adjusted with Tris) bubbled with 100% O<sub>2</sub> at room temperature. The cannulated perfused heart was submerged in the Tyrode solution, the LV was opened, and trabeculae (typically located around the papillary muscles) were dissected. A geometrically uniform and suitable LV trabecula was then transferred to the microcalorimeter and mounted between two platinum hooks, one connected to a force transducer at the downstream end and the other attached to a length-control motor at the upstream end (Taberner et al., 2011). The trabecula was superfused with oxygenated Tyrode solution (with 1.5 mmol/liter CaCl<sub>2</sub> and in the absence of 2,3-butanedione monoxime) at a rate of 0.5–0.7 μl s<sup>-1</sup>.

### Mechano-energetics experimental protocols

Once mounted in the microcalorimeter, the trabecula was electrically stimulated at 3 Hz using platinum electrodes for at least 1 h to achieve mechanical and thermal steady-states before it was incrementally stretched to optimal length to achieve maximal developed isometric force ( $L_0$ ). The work-loop calorimeter was enclosed within a light-proof, thermally insulated hood to diminish external optical and thermal disturbances, with ambient temperature within the enclosure maintained at 32°C. Experiments commenced when a stable thermal environment, and steady-states of force and heat rate production of the trabecula, were achieved. The trabecula was subjected to a work-loop protocol, and an isometric length-change protocol, as illustrated in Fig. 2 A and Fig. 4 A. Briefly, the work-loop protocol involved a series of work-loop contractions at progressively diminishing afterloads, with the minimum afterload in

the vicinity of passive force (interspersed by isometric contractions between each afterload selection). The length-change protocol involved a series of isometric contractions at progressively diminishing muscle lengths in six steps, commencing at  $L_0$  and proceeding to the minimum length that produced near zero developed force (0.77  $L_0$ ). These length-change steps provide assessment of mechanics over the full working range of the trabeculae, and the consequent change in active stress is comparable to previous studies (ter Keurs et al., 1980; de Tombe and ter Keurs, 1991; Kentish et al., 1986).

Following completion of the two protocols, stimulation was turned off, and the trabecula remained at its quiescent state to facilitate quantification of two sources of heat artifact. First, to correct for the heat artifact induced by the cyclic movement of the upstream hook during work-loop contractions, heat was measured with the length control motor oscillating the trabecula mounting hook at 3 Hz over a distance equivalent to the extent of muscle shortening achieved at the lowest afterload. This heat artifact related to the movement of the mounting hook was ~2% of the measured heat signal. Second, the trabecula was removed from the microcalorimeter, and the heat artifact resulting from electrical stimulation at 3 Hz was measured (<10% of the measured heat signal).

### Trabecula dimensions

In total,  $n = 12$  trabeculae per group were studied in the microcalorimeter. Muscle length and width at  $L_0$  were measured using a microscope graticule. Average trabecula dimensions did not differ between the control and hypertrophy groups, respectively, in diameter (280 μm ± 23 μm versus 295 μm ± 20 μm), length (2.26 mm ± 0.20 mm versus 2.51 mm ± 0.24 mm), cross-sectional area (0.066 mm<sup>2</sup> ± 0.010 mm<sup>2</sup> versus 0.072 mm<sup>2</sup> ± 0.010 mm<sup>2</sup>), and volume (0.155 mm<sup>3</sup> ± 0.029 mm<sup>3</sup> versus 0.196 mm<sup>3</sup> ± 0.039 mm<sup>3</sup>).

### Mechano-energetics data analysis

Simultaneous measurements of force, length, and rate of heat output were acquired using LabVIEW software (National Instruments) and analyzed offline using a custom-written MATLAB program (MathWorks). The rate of heat production (in units of W) was converted to heat per twitch by dividing by the stimulus frequency (3 Hz), normalized to muscle volume, and expressed in units of kJ m<sup>-3</sup>. Activation heat was estimated by our previously validated approach (Pham et al., 2017) of determining the intercept of the heat-stress relation where force production is negligible. Cross-bridge heat was determined by subtracting activation heat from active heat. Muscle force (in units of N) was converted to stress (in units of kPa) by dividing by muscle cross-sectional area. The maximum rates of rise and fall of trabecula stress (±dS/dt, in units of MPa s<sup>-1</sup>) were computed from the ascending and descending limbs of the twitch, respectively. The duration of the stress rise (contraction) was quantified as the time from 5% rise to peak stress. The duration of the stress fall (relaxation) was quantified as the time from peak stress to 95% decay of the stress signal. Muscle length was expressed relative to optimal muscle length ( $L/L_0$ ).

In the work-loop protocol, afterload was defined as the stress at which the muscle transitioned from the isometric phase to isotonic shortening, whereas active afterload was defined as the



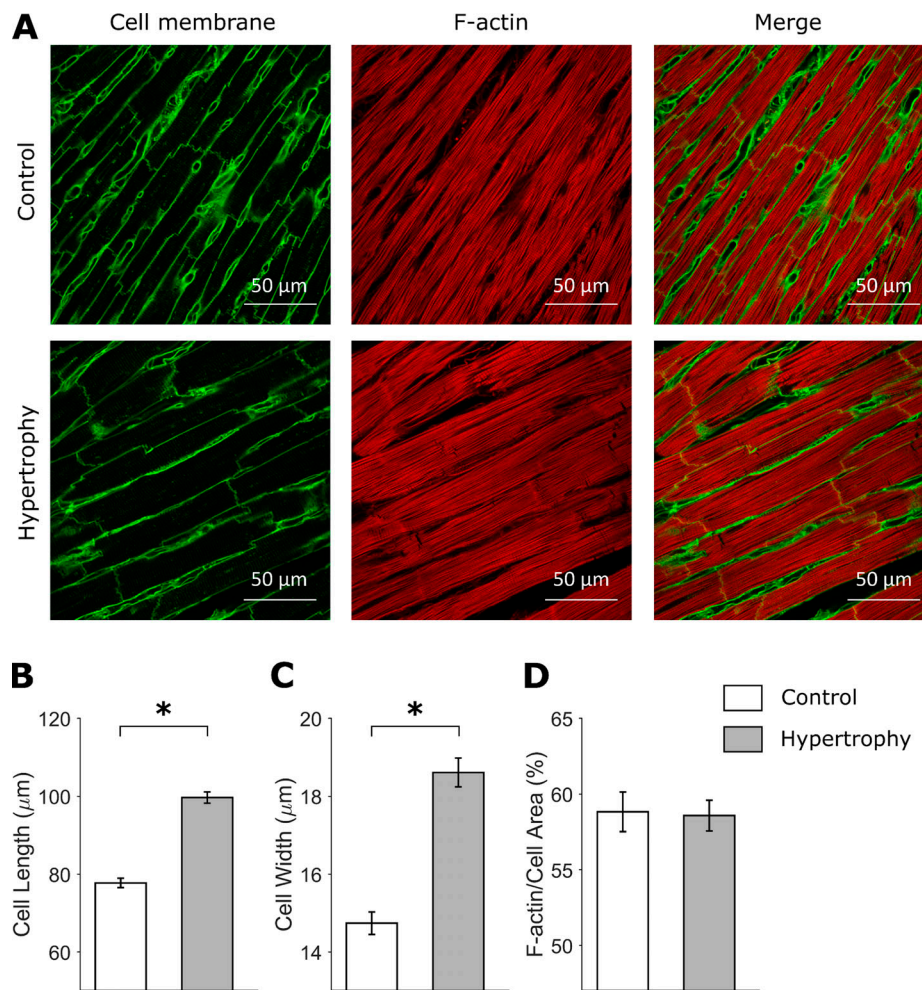


**Figure 1. Cardiomyocyte hypertrophy.** (A) Representative confocal images of WGA- and phalloidin-stained LV sections. (B and C) Cardiomyocyte length (B) and width (C; control:  $n = 257$  cells; hypertrophy:  $n = 237$  cells; from five to eight images per heart,  $n = 3$  hearts per group). (D) Percentage of F-actin area (control:  $n = 24$  cells, hypertrophy:  $n = 26$  cells; from two or three images per heart,  $n = 3$  hearts per group). Graphs show mean  $\pm$  standard error. Data analyzed by nested ANOVA; \*,  $P < 0.05$ .

difference between afterload and passive stress. The width of the loop was quantified as the extent of muscle shortening, and the area within the loop quantified the mechanical work (in units of  $\text{kJ m}^{-3}$ ) performed by the muscle. The maximum velocity of muscle shortening for each work-loop was computed from the length-time trace during the isotonic shortening phase. Its value was normalized to muscle length and was thus expressed in units of  $\text{s}^{-1}$ . Power of shortening (in units of  $\text{kW m}^{-3}$ ) was defined as the product of velocity of shortening and active afterload.

To account for the slow time-drift of the temperature inside the insulated enclosure over the duration of the experiment, baseline heat rate was recorded from the muscle in a quiescent state between interventions with the stimulation halted. These baseline heat data were fitted with a polynomial function and subtracted from the active heat values.

#### Statistical analyses

Variables were plotted as functions of either relative muscle length or stress, and data were fitted using polynomial regressions. Regression lines were obtained for each trabecula,

and the difference between groups was statistically analyzed using a random coefficient model (SAS Institute Inc.; Feldman, 1988). A Student's  $t$  test or nested ANOVA was used for comparison of two groups where appropriate. A  $P$  value of  $<0.05$  was taken as significance in the difference between the two groups.

## Results

### Relative cardiac hypertrophy, increased cardiomyocyte dimensions, and unchanged percentage of F-actin area

Rats with normotensive cardiac hypertrophy exhibited lower body mass and tibial length relative to control rats (Table 1). Although nonnormalized heart mass and ventricular mass were similar between groups, relative cardiac hypertrophy was confirmed when heart mass and ventricular mass were normalized to body mass (Table 1). Hypertrophy was evident at the cellular level by evaluation of cardiomyocyte dimensions in fixed LV sections stained with WGA, revealing 28% increased ( $P < 0.0001$ ) cardiomyocyte length and 26% increased ( $P < 0.0001$ ) cardiomyocyte width (Fig. 1, A–C). The proportional area of

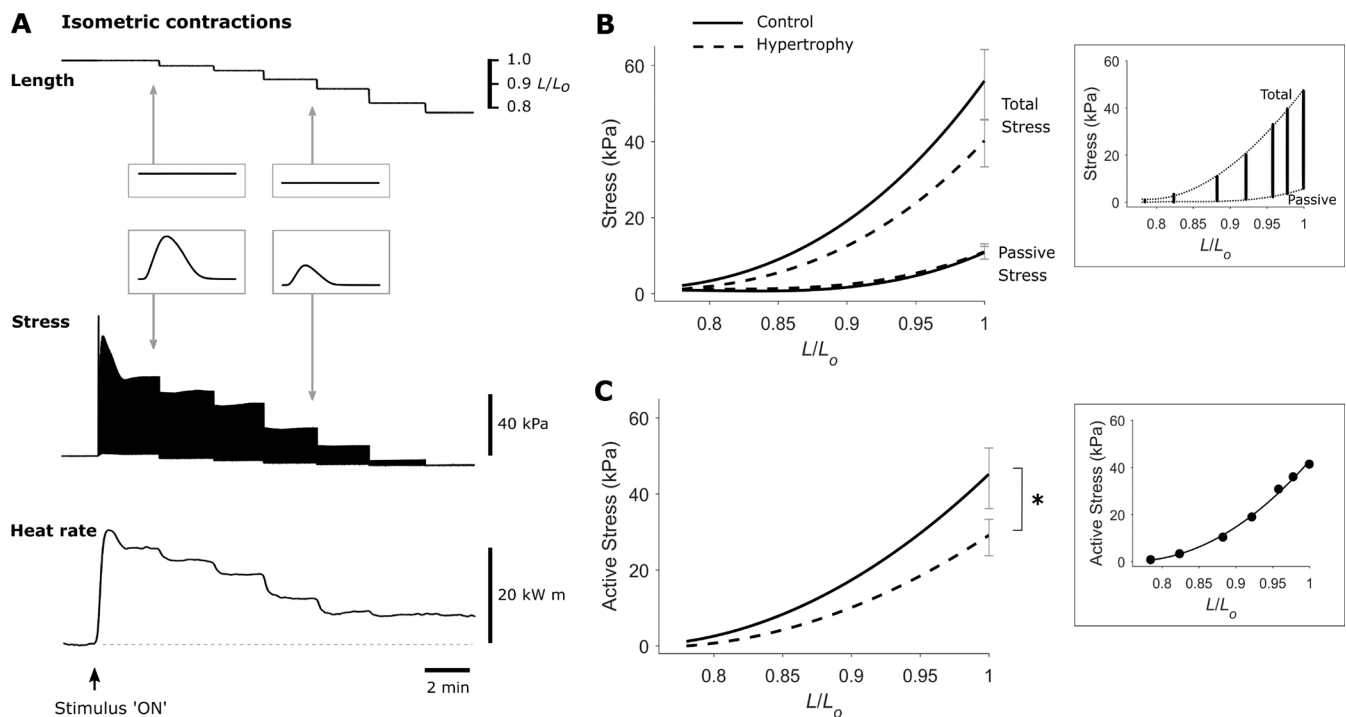


Figure 2. **Impaired steady-state isometric active stress production in trabeculae from rats with cardiac hypertrophy.** (A) Exemplar recordings from a trabecula show simultaneous measurement of length, stress, and heat rate during the isometric length-change protocol. The isometric length-change protocol involved a series of 3-Hz isometric contractions at progressively diminishing muscle lengths, commencing at  $L_0$  and proceeding to the minimum length (around  $0.77 L_0$ ), which produced near-zero developed stress. A single twitch at steady-state is shown in each inset. Baseline heat rate is indicated by the horizontal broken line. (B) Average total and passive stress-length relations of control (solid lines) and hypertrophic rat (broken lines) trabeculae,  $n = 12$ . Data from an exemplar trabecula are shown in the inset, and the end-systolic (total) and end-diastolic (passive) points are fitted with cubic polynomial functions (dotted lines). (C) Average active stress-length relations of control (solid line) and hypertrophic rat (broken line) trabeculae, calculated by subtracting the passive stress from total stress,  $n = 12$ . Data from an exemplar trabecula are shown in the inset and fitted with cubic regression. The SEM for each relation is shown at the maximal stress obtained at  $L_0$ . The difference between average regression lines was analyzed by the random coefficient model; \*,  $P < 0.05$ .

F-actin determined by analysis of phalloidin-stained LV sections was similar between groups (Fig. 1 D).

#### Functional impairment evident in isometric contractions

Cardiac mechanical performance was evaluated in isolated LV trabeculae from control and hypertrophic rats. The trabeculae were subjected to a series of isometric contractions at progressively diminishing muscle lengths (from  $L_0$  to  $\sim 0.77 L_0$ ) with simultaneous measurement of stress and rate of heat output (Fig. 2 A). The data from the isometric length-change protocol are plotted in Figs. 2 and 3. Total stress and passive stress were not statistically different between groups (Fig. 2 B). The active stress-length relationship was significantly lower ( $P = 0.0345$ ) in hypertrophic rat trabeculae relative to controls (Fig. 2 C).

The time to 95% twitch relaxation (twitch fall), as a function of relative active stress, was statistically different ( $P = 0.0021$ ) between groups, showing prolonged relaxation in the cardiac hypertrophy group (Fig. 3 A). There were no statistically significant differences between groups in the time to peak stress (twitch rise, Fig. 3 A), or in the rates of rise and fall, as functions of relative active stress (Fig. 3 B).

#### Impaired shortening during work-loop contractions

To simulate the pressure-volume loops of the intact heart, trabeculae were subjected to stress-length work-loops at eight

different afterloads. Representative traces are presented in Fig. 4, A–D, to illustrate the experimental records arising from the work-loop protocol. The stress and length profiles at each of the eight afterloads from an exemplar trabecula are superimposed in Fig. 4, B and C, with the corresponding stress-length work-loops presented in Fig. 4 D. All work-loop contractions commenced at an end-diastolic muscle length of  $L_0$ . The maximum afterload was defined by the isometric contraction, and the minimum afterload was performed by imposing an afterload value in the vicinity of passive stress. The width of each work-loop represents the extent of muscle shortening, and is plotted in Fig. 5 A. The extent of shortening, velocity of shortening, and power of shortening are plotted as functions of relative active stress (Fig. 5, A–C). In all three measures of the kinetics of shortening, the relations were significantly lower in the hypertrophic rat group compared with controls ( $P = 0.0254$ ,  $0.0002$ , and  $0.0096$ , respectively, for the significant difference between the two curves in each panel of Fig. 5). To determine whether reduced shortening kinetics were associated with a difference in the MHC isoforms, mRNA expression of  $\alpha$ -MHC and  $\beta$ -MHC was assessed in LV tissues, with the data expressed as a fold-change with respect to the control rats (Fig. 5 D). Rats with cardiac hypertrophy exhibited greater  $\beta$ -MHC expression ( $P = 0.0046$ ), but with no change in  $\alpha$ -MHC

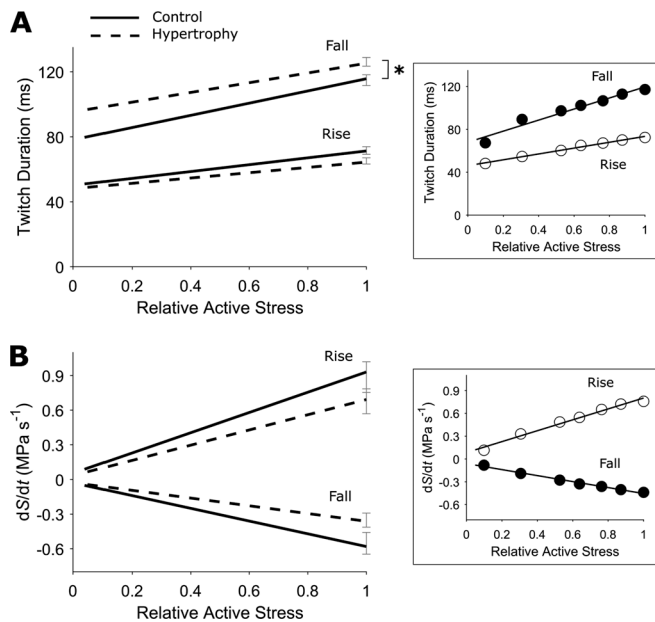


Figure 3. **Prolonged trabecula isometric stress duration.** (A) The durations of isometric twitch “rise” (time from 5% rise to peak stress) and “fall” (time from peak stress to 95% relaxation) were quantified and presented as relations of active stress (relative to peak stress at  $L_0$ ). (B) The rates of rise and fall of isometric twitch denote, respectively, the maximum slopes of the ascending (+dS/dt) and descending (–dS/dt) portions of the twitch, and are presented as relations of active stress (relative to peak stress at  $L_0$ ). In both panels, the SEM for each relation is shown at peak active stress obtained at  $L_0$ . Control rat (solid lines), hypertrophic rat (broken lines),  $n = 12$  trabeculae. The difference between regression lines was analyzed by the random coefficient model; \*,  $P < 0.05$ . In the inset, data from an exemplar trabecula are shown, and fitted using linear regression.

expression, leading to greater proportion of  $\beta$ -MHC ( $P = 0.0108$ ).

#### Lower energy expenditure related to cardiac activation and cross-bridge cycling

Energy expenditure was determined by measurement of heat output from the trabeculae during the series of isometric and work-loop contractions (as shown in Fig. 2 A and Fig. 4 A). Active heat output arising from isometric contractions at varying muscle lengths was plotted as a function of active stress in Fig. 6 A. The isometric heat-stress relation was significantly lower ( $P = 0.0168$ ) in hypertrophic rat trabeculae relative to controls. Peak isometric active heat was lower in the cardiac hypertrophy group (control:  $10.9 \pm 1.6 \text{ kJ m}^{-3}$  versus hypertrophy:  $5.5 \pm 0.8 \text{ kJ m}^{-3}$ ;  $P = 0.0077$ ). Similarly, the heat-intercept was also lower ( $P = 0.0166$ ) in the hypertrophic rat trabeculae (Fig. 6 A), indicating lower energy expended on non-cross-bridge ATP hydrolysis, i.e.,  $\text{Ca}^{2+}$  cycling (activation heat, control:  $3.0 \pm 0.2 \text{ kJ m}^{-3}$  versus hypertrophy:  $1.4 \pm 0.2 \text{ kJ m}^{-3}$ ; Fig. 7, A and C). The energy expenditure related to cross-bridge cycling was determined by subtracting activation heat from total active heat for the series of isometric and work-loop contractions. Isometric cross-bridge energy expenditure was similar between groups, but significantly lower ( $P = 0.0176$ ) cross-bridge heat was evident during work-loop contractions in trabeculae from

hypertrophic rodents (Fig. 6 B). The difference between cross-bridge heat during isometric and work-loop contractions is termed shortening heat. Lower work-loop cross-bridge energy expenditure in hypertrophic rats was consistent with a non-significant trend for lower peak shortening heat in this group (Fig. 6 E;  $P = 0.1272$ ). The inverse slope of the isometric heat-stress relation was not different between groups, indicating no difference in the cross-bridge economy (Fig. 6 D). Cardiac SERCA2a protein expression was not significantly different between groups (Fig. 6 F).

#### Preserved mechanical and cross-bridge efficiencies

To evaluate the mechano-energetics of hypertrophic rat trabeculae, simultaneous measurement of work and heat output were recorded to calculate enthalpy (sum of mechanical work and heat) and mechanical efficiency (ratio of work and enthalpy) for a range of afterloads. These variables were plotted as functions of relative afterload during the work-loop protocol in Fig. 7. In hypertrophic rat trabeculae, lower work output (Fig. 7 A;  $P = 0.0035$ ) was paralleled by lower enthalpy output (Fig. 7 B;  $P = 0.0017$ ) and, as such, there was no difference in mechanical efficiency (peak value: control,  $13.1 \pm 1.2\%$  versus hypertrophy,  $13.4 \pm 1.0\%$ ; Fig. 7 C).

Cross-bridge heat and cross-bridge enthalpy (the sum of mechanical work and cross-bridge heat) were significantly lower in hypertrophic rat trabeculae relative to controls (Fig. 8 A;  $P = 0.0176$  and  $0.0017$ , respectively). The ratio of work and cross-bridge enthalpy yields a measure of cross-bridge efficiency, which was not different between groups (peak cross-bridge efficiency: control,  $22.9 \pm 2.0\%$  versus hypertrophy,  $21.9 \pm 2.1\%$ ; Fig. 8 B).

#### Discussion

This study provides the first comprehensive examination of cardiac mechano-energetic function associated with primary cardiac hypertrophy. In LV trabeculae isolated from rats with normotensive cardiac hypertrophy, we have examined mechanical and energetic performance using both isometric and work-loop contraction protocols. Impaired mechanical performance is evident in trabeculae from hypertrophic rats, characterized by lower isometric stress production, lower extent of shortening, and slower kinetics of shortening, resulting in lower mechanical work output. The energy expenditure attributed to both cardiac activation (predominantly the ATP hydrolysis related to  $\text{Ca}^{2+}$  cycling) and cross-bridge cycling is lower in hypertrophic rat trabeculae. Mechanical and cross-bridge efficiencies are preserved. Collectively these findings demonstrate that cardiac functional impairment is evident in trabeculae from rats with primary cardiomyocyte hypertrophy, with preservation of cardiac efficiency.

#### Primary cardiac hypertrophy is associated with disturbances in cardiac muscle mechanics

The rat model employed in this study is a polygenic model of progressive cardiac hypertrophy independent of blood pressure hemodynamic loading (Harrap et al., 2002). In the present study, we have evaluated cardiac trabeculae from hypertrophic

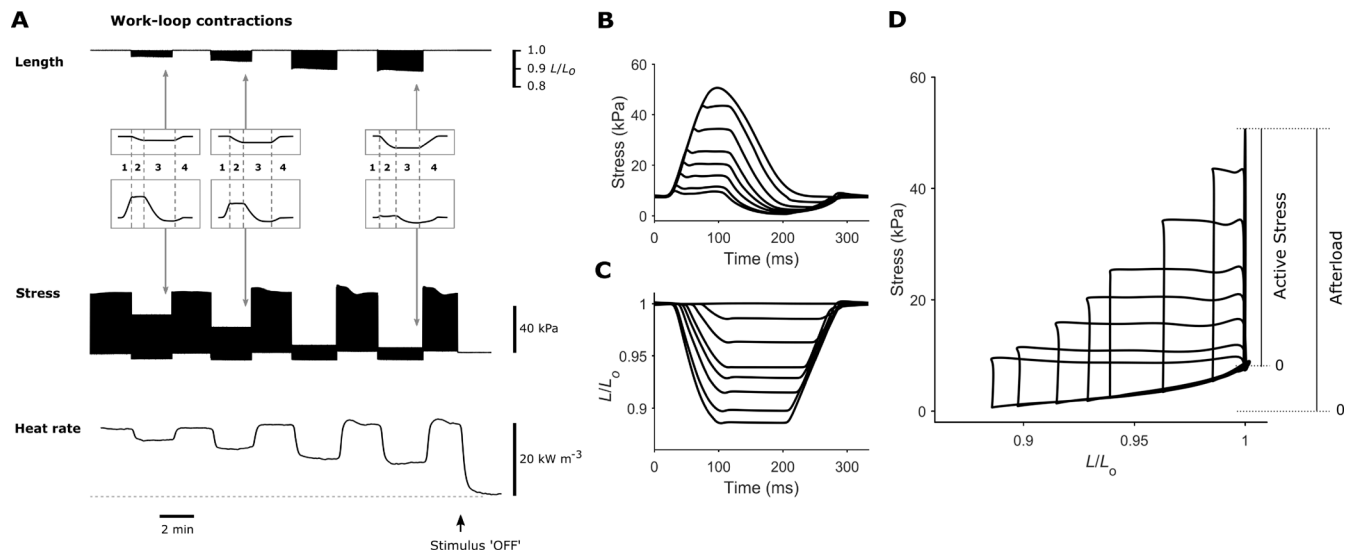


Figure 4. **Trabecula stress-length work-loops at steady-state.** (A) Exemplar recordings from a trabecula show simultaneous measurement of length, stress, and heat rate. In the work-loop protocol, muscle length was set at  $L_0$  (preload), and the muscle was subjected to a series of 3-Hz work-loop contractions at progressively diminishing afterloads, with the minimum afterload in the vicinity of passive force. Contractions at each afterload were interspersed by isometric contractions. A single work-loop twitch at steady-state is shown in each inset, where the four phases of the work-loop contraction are (1) isometric contraction, (2) isotonic shortening, (3) isometric relaxation, and (4) relengthening. Baseline heat rate is indicated by the horizontal broken line. (B) Twitches from an exemplar trabecula undergoing eight different afterloaded work-loop contractions superimposed. A work-loop contraction of a sufficiently high afterload, i.e., greater than the peak isometric stress, essentially resulted in an isometric twitch. The lowest achievable afterload was in the vicinity of the passive stress. (C) The changes of muscle length corresponding to each of the eight afterloaded work-loop contractions in B are superimposed. (D) A parametric plot of the stress in B and the length in C reveals the eight afterloaded work-loops. Active stress is the stress above passive stress, whereas afterload occupies the range of total stress.

rats at a young adult time point (12 wk old) to define the early characteristics of disease. At this early age, we confirm that relative cardiac hypertrophy is detectable (heart weights normalized to body weight), coincident with increased cardiomyocyte dimensions. These findings are consistent with our previous report demonstrating that the extent of cardiac hypertrophy, relative to controls, was most prominent at 12 wk of age in this model (Porrello et al., 2009a). In this rat model, primary cardiac hypertrophy is characterized by increased myocyte length and width. These findings contrast with the conventional traits of volume overload-induced increased myocyte length (with normal width), or pressure overload-induced increased myocyte width (with normal length). Thus, this model demonstrates that primary hypertrophy is distinctive and provides an opportunity for investigation of cardiac hypertrophy in the absence of external cardiac stressors. The etiology of cardiac hypertrophy in this rat model originates with elevated cell death and early terminal differentiation of cardiomyocytes at the neonatal stage (Porrello et al., 2009a). In the present study, cardiomyocyte hypertrophy was evident despite no change in heart mass, consistent with the contention that early terminal differentiation of myocytes in the neonate translates to fewer cardiomyocytes in the adult heart. Lower expression of the angiotensin-II 1a receptor has been reported, coincident with a threefold increase in the levels of pathological hypertrophy markers,  $\beta$ -MHC, cardiac atrial natriuretic peptide, and b-type natriuretic peptide (Porrello et al., 2009a). The findings of the present study demonstrate that a marked disturbance in cardiac mechanics is associated with primary cardiac hypertrophy in the early adult

stage of disease progression. Hypertrophic rat trabeculae operate at a lower level of mechanical performance relative to controls, with lower isometric stress production, extent of shortening, and work output. Lower force production in the hypertrophic rats is not explained by differences in myofibrillar density, as the percentage of F-actin area (relative to cell area) was similar to the control group. The hypertrophic rat trabeculae also exhibited slower contraction kinetics as evidenced by prolonged duration of the diastolic period of the isometric stress profile and slower work-loop shortening velocity. The underlying mechanism of impaired kinetics of contraction in this model may involve changes in myofilament gene expression, consistent with our finding of higher expression of the  $\beta$ -MHC isoform. A switch from  $\alpha$ -MHC to  $\beta$ -MHC is commonly observed in cardiac pathological states and is well established to be linked with slower shortening kinetics (Fitzsimons et al., 1998). However, species differences in the proportion of  $\alpha$ - to  $\beta$ -MHC (~75%  $\alpha$ -MHC in rodents [Cappelli et al., 1989] versus ~7%  $\alpha$ -MHC in humans [Miyata et al., 2000]) should be noted, and an increase in the  $\beta$ - to  $\alpha$ -MHC isoform ratio may have less impact in the clinical context. Our previous studies have reported similar findings of reduced mechanical performance in trabeculae from rats with hypertensive cardiac hypertrophy (SHRs; Han et al., 2014). However, the underlying mechanisms appear to be different, as discussed below.

#### Disturbed cardiac mechanics and preserved mechanical efficiency are distinct outcomes of primary cardiac hypertrophy

In the present study, mechanical efficiency is preserved in LV trabeculae from rats with primary cardiac hypertrophy,



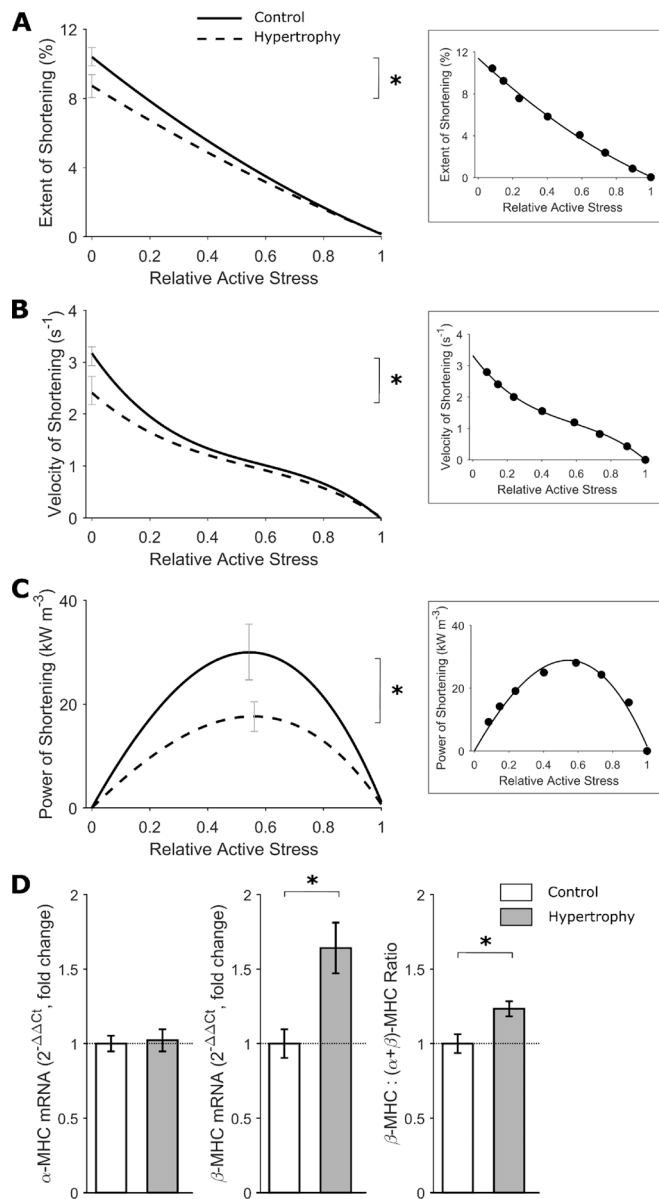


**Figure 5. Slower trabecula shortening kinetics during work-loop contractions.** (A) Extent of shortening signifies the width of the work-loop (Fig. 6 C), and is expressed as a percentage of  $L_0$ . The average relations of extent of shortening and active stress (relative to peak stress at  $L_0$ ) were fitted using quadratic regression. (B) Velocity of shortening was quantified as the slope of the length trace at the shortening phase of the work-loop (Fig. 6 A). The average relations of velocity of shortening and active stress (relative to peak stress at  $L_0$ ) were fitted using cubic regression. (C) Power of shortening was quantified as the product of velocity of shortening and active stress. The average relations of power of shortening and active stress (relative to peak stress at  $L_0$ ) were fitted using cubic regression with both variables fixed at zero at the origin. (D) MHC mRNA expression (measured by the  $2^{-\Delta\Delta Ct}$  method) of the  $\alpha$  and  $\beta$  isoforms. Data were expressed as fold change relative to the control group ( $n = 9$  per group). In A–C, control rat (solid lines), hypertrophic rat (broken lines),  $n = 12$  trabeculae. SEM is superimposed at peak values for each relation. The difference between regression lines was analyzed by the random coefficient model; \*,  $P < 0.05$ . Insets in each panel show data from an exemplar trabecula. In D, graphs show mean  $\pm$  standard error. Data analyzed by Student's  $t$  test; \*,  $P < 0.05$ .

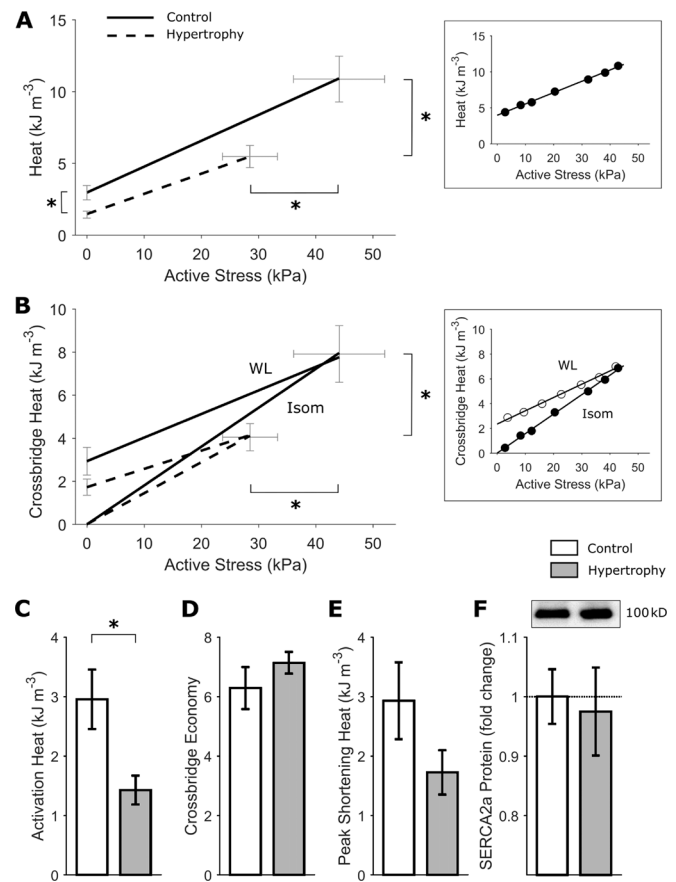


**Figure 6. Lower energy expenditure related to cardiac activation and cross-bridge cycling.** (A) Average heat-stress relation from the isometric length-change protocol. Control rat (solid line), hypertrophic rat (broken line).  $n = 12$  trabeculae. SEM for the relation is shown at peak active stress obtained at  $L_0$  and at the heat-intercept. The inset shows data from an exemplar trabecula, fitted using linear regression. (B) Cross-bridge heat under isometric contractions (Isom) and under work-loop contractions (WL). Control rat (solid line), hypertrophic rat (broken line).  $n = 12$  trabeculae. SEM for the relation is shown at peak active stress obtained at  $L_0$  and at the cross-bridge heat-intercept. The inset shows data from the same exemplar trabecula as in A, fitted using linear regression. (C) The heat-intercept of the heat-stress relation in A quantifies the activation heat, defined as the energy expenditure from activating the contractile unit, arising from the energetic cost of cellular cycling of  $Ca^{2+}$ .  $n = 12$  trabeculae. (D) The reciprocal of the slope of the heat-stress relation in A gives a measure of cross-bridge economy.  $n = 12$  trabeculae. (E) Peak shortening heat, estimated from the cross-bridge heat-intercept in B under the work-loop contraction, is not significantly different between groups. (F) SERCA2a protein expression in LV tissues from control and hypertrophic rats ( $n = 9$  per group). (C and D) Mean  $\pm$  standard error, analyzed by the random coefficient model of the heat-stress intercept and slope of the regression lines in A. (F) Mean  $\pm$  standard error, analyzed by Student's  $t$  test. \*,  $P < 0.05$ .

contrasting with our previous studies in hypertensive hypertrophic rats, where mechanical efficiency is reduced (Han et al., 2014; Pham et al., 2018). These findings highlight that caution is needed when attributing altered mechano-energetics to myocardial hypertrophy. In the SHR, where hypertrophy is secondary to systemic hypertension, reduced mechanical efficiency is a consequence of impaired cross-bridge cycling with normal energy expenditure (Han et al., 2014). In the pulmonary



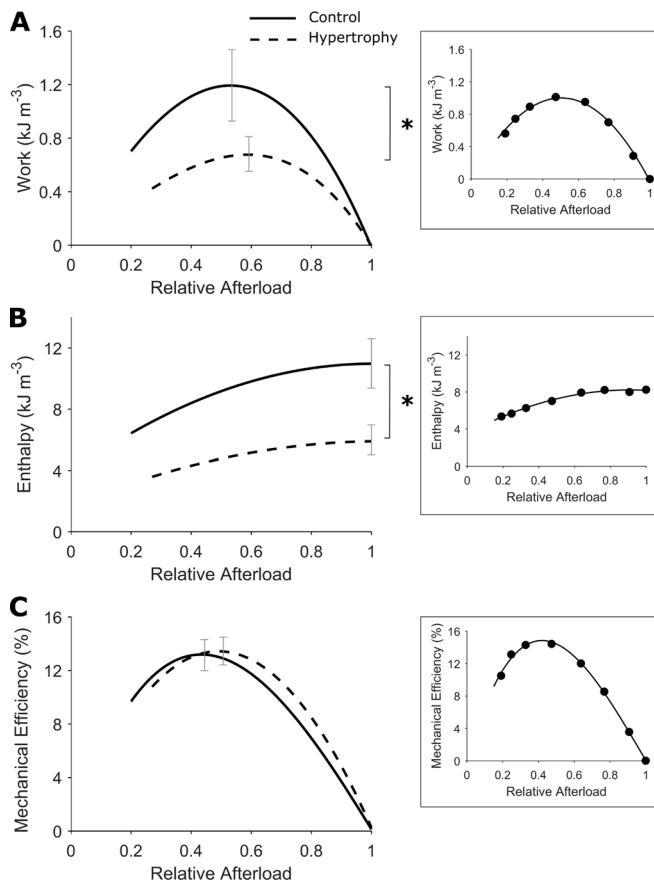


**Figure 7. Lower trabecula work output and enthalpy but preserved mechanical efficiency.** (A) Mechanical work output was quantified as the integral of stress with respect to length over a work-loop twitch, which denotes the area within the work-loop. The average relations of work and afterload (relative to peak total stress obtained at  $L_0$ ) were fitted using cubic regression with both variables constrained at the origin. The regression lines are drawn to commence at relative passive stress. (B) Enthalpy is the sum of work and heat. The average relations of enthalpy and afterload (relative to peak total stress obtained at  $L_0$ ) were fitted using quadratic regression. (C) Mechanical efficiency is the ratio of work to enthalpy. The average relations of mechanical efficiency and afterload (relative to peak total stress obtained at  $L_0$ ) were fitted using cubic regression with both variables constrained at the origin. The regression lines are drawn to commence at relative passive stress. Control rat (solid lines), hypertrophic rat (broken lines),  $n = 12$  trabeculae. SEM is superimposed at peak values for each dependent variable. The difference between regression lines was analyzed by the random coefficient model; \*,  $P < 0.05$ . Insets in each panel show data from an exemplar trabecula.

hypertensive rat, reduced mechanical efficiency is a consequence of increased  $\text{Ca}^{2+}$  cycling-related energy expenditure (Pham et al., 2018). In the present study, with primary cardiac hypertrophy, both work output and energy expenditure were lowered simultaneously, such that mechanical efficiency was preserved.

Lower active energy expenditure observed in the hypertrophic rat trabeculae in this study arises from two sources. First is the lower energy cost of cardiac activation, as estimated by the rate of heat production in the absence of measurable force (Johnston et al., 2015). The heat of activation reflects the ATP consumption required to restore ionic homeostasis following a

contraction, and is attributed primarily to the events associated with the cycling of  $\text{Ca}^{2+}$  (the metabolic cost of restoring ion gradients for the action potential is usually considered to be negligible; Loiselle, 1987). Given that activation heat has been shown to predominantly reflect ATP hydrolysis by the SERCA, with some contribution from the sarcolemmal  $\text{Ca}^{2+}$  adenosine triphosphatase (ATPase) and  $\text{Na}^+$ - $\text{K}^+$  ATPase (Gibbs et al., 1988), it could be anticipated that  $\text{Ca}^{2+}$  cycling through SERCA and  $\text{Ca}^{2+}$  ATPase is lower in this setting of primary cardiac hypertrophy. In the present study, cardiac SERCA2a protein expression was similar in hypertrophic and control rats, indicating that lower activation heat (suggesting lower  $\text{Ca}^{2+}$  cycling) is not explained by a deficiency in SERCA protein content. These findings provide the basis for further investigation to evaluate the rate of SERCA activity and fully characterize the  $\text{Ca}^{2+}$  handling changes in this hypertrophic rat model. The finding that activation heat is lower in the hypertrophy group is consistent with decreased activity of SERCA and  $\text{Na}^+$ - $\text{K}^+$  ATPase commonly observed in cardiac hypertrophy settings (Pogwizd et al., 2003). Increased NCX activity has also been reported with cardiac hypertrophy (Pogwizd et al., 2003); however, NCX-mediated  $\text{Ca}^{2+}$  removal flux has a relatively small influence on activation heat. In the rat heart, 92% of the  $\text{Ca}^{2+}$  removal is achieved by SERCA, with 7% from the coupling between  $\text{Na}^+$ - $\text{K}^+$  ATPase and NCX, and the remaining 1% by the sarcolemmal  $\text{Ca}^{2+}$  ATPase and mitochondrial  $\text{Ca}^{2+}$  uniporter (Bers, 2002). Given that SERCA cycles twice as many  $\text{Ca}^{2+}$  for each ATP hydrolyzed as the other  $\text{Ca}^{2+}$  transporters, these contributions amount to 85% ATP hydrolysis by SERCA and 13% ATP hydrolysis by  $\text{Na}^+$ - $\text{K}^+$  ATPase in concert with NCX. Using our values of activation heat, the number of  $\text{Ca}^{2+}$  ions cycled per twitch can be estimated (Widén and Barclay, 2006; Han et al., 2010). Activation heat values for control and hypertrophy rats correspond to estimates of  $6.56 \times 10^{12}$  and  $4.00 \times 10^{12}$   $\text{Ca}^{2+}$  cycled per twitch (per trabecula), respectively. The second source of lower active energy expenditure in trabeculae from rats with primary hypertrophy is related to reduced cross-bridge cycling (evidenced by lower cross-bridge heat), indicative of fewer ATPs hydrolyzed by myosin ATPase. Given that cross-bridge efficiency and economy were unchanged, lower force production may be related to impaired  $\text{Ca}^{2+}$  handling, and the findings from the present study provide the lead for future studies directly measuring  $\text{Ca}^{2+}$  transients and underlying molecular mechanisms in this model.

Interestingly, the relation between cross-bridge heat and active stress was detected to be significantly lower in hypertrophic rats when derived from work-loop contractions, but unchanged in isometric contractions. This finding suggests that a component of cross-bridge energy expenditure associated with the action of muscle shortening may play a role. Shortening heat is determined by the difference between work-loop and isometric cross-bridge heat, and was slightly (albeit not statistically significantly) decreased in the hypertrophy group. Shortening heat is a well-known concept in the skeletal muscle field, yet was only recently demonstrated to exist in cardiac muscle (Tran et al., 2017, 2020). The slightly lower shortening heat in trabeculae from hypertrophic rats is consistent with the observed lower extent, and velocity, of shortening.

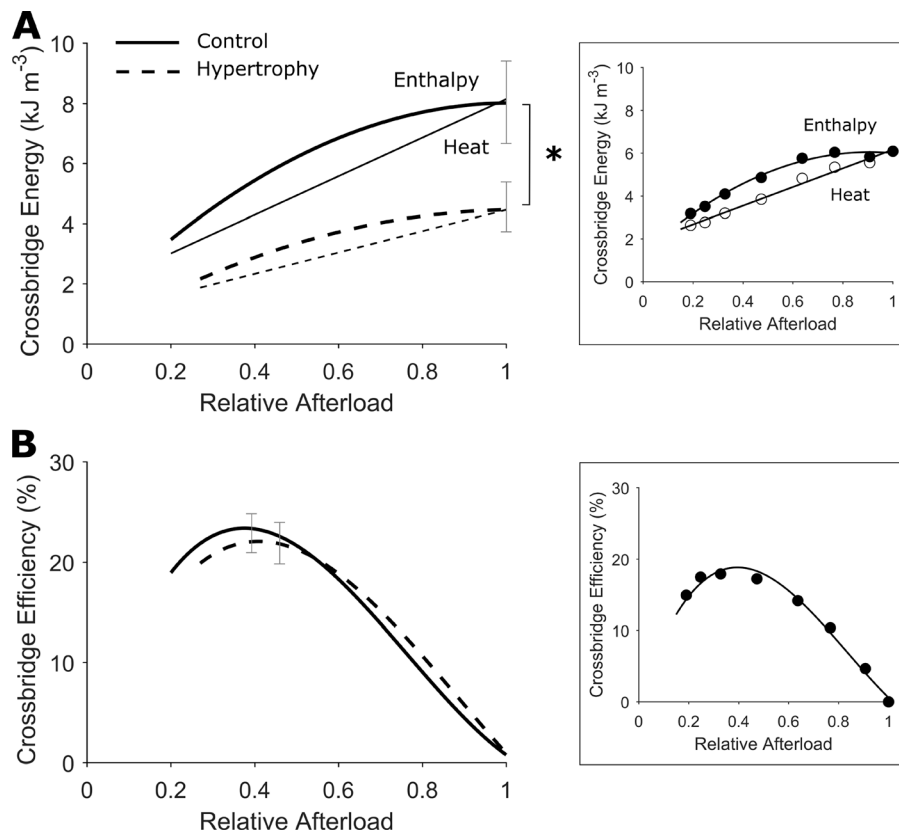


Figure 8. **Lower trabecula cross-bridge enthalpy and preserved cross-bridge efficiency.**

(A) Cross-bridge heat was quantified by subtracting activation heat (estimated from the y intercept of the heat-stress relation in Fig. 5 A) from active heat. Cross-bridge enthalpy is thus the sum of cross-bridge heat and work output. The average relations of cross-bridge heat and afterload (relative to peak total stress obtained at  $L_0$ ) were fitted using linear regression (thin lines). The average relations of cross-bridge enthalpy and relative afterload were fitted using quadratic regression (thick lines). (B) Cross-bridge efficiency is the ratio of work to cross-bridge enthalpy. The average relations of cross-bridge efficiency and afterload (relative to peak total stress obtained at  $L_0$ ) were fitted using quadratic cubic regression with both variables constrained at the origin. The regression lines are drawn to commence at relative passive stress. Control rat (solid lines), hypertrophic rat (broken lines),  $n = 12$  trabeculae. SEM is superimposed at peak values for each dependent variable. The difference between regression lines was analyzed by the random coefficient model; \*,  $P < 0.05$ . Insets in each panel show data from an exemplar trabecula.

Metabolic disturbances are commonly observed in cardiac pathological settings, and it has been previously demonstrated that mitochondrial ATP production is lower in hypertensive cardiac hypertrophy (SHRs; Hickey et al., 2009; Power et al., 2016). Whether metabolic dysfunction is evident in a primary hypertrophy setting has not been established. An impairment in ATP production would be expected to limit ATP supply to cellular ATPases and may contribute to the observed reduced activation heat and suppressed cross-bridge heat and force output in the trabeculae from hypertrophic rats in the present study. Further investigation into mitochondrial bioenergetics, distribution, and morphology in settings of primary hypertrophy would test this hypothesis.

#### Comparison with clinical cardiac hypertrophy and myocardial efficiency

Multiple regression analyses have revealed that increased LV size is linked with heart failure progression, after adjusting for variation in blood pressure and other comorbidities (Levy et al., 1990). The animal model employed in the present study provides a unique experimental setting for direct investigation into the effects of cardiac hypertrophy on mechano-energetics, in the absence of blood pressure increase. Clinical studies of acquired cardiac hypertrophy are often complicated by a plethora of comorbidities, including hypertension. Cardiac energetics studies directly comparing patients with acquired hypertrophy in the presence and absence of hypertension are lacking. In patients with cardiac hypertrophy secondary to systemic (Laine et al., 1999) and pulmonary (Wong et al., 2011) hypertension,

myocardial efficiency is reduced due to impaired mechanical work with unchanged myocardial oxygen consumption.

Although the underlying etiology is distinct, comparison of our findings with those from patients with inherited hypertrophic cardiomyopathy is worth noting, as this is commonly a hypertrophic setting where blood pressure is normal (Antunes and Scudeler, 2020). In clinical studies investigating patients with familial hypertrophic cardiomyopathy, lower myocardial efficiency has also been reported. In these patients, external work is unchanged, but myocardial O<sub>2</sub> consumption is increased, evaluated by [<sup>14</sup>C]-acetate positron emission tomography and cardiovascular magnetic resonance imaging (Güçlü et al., 2017). Lower efficiency in this context has been attributed to a higher energy cost of contraction due to mutations in the myofilaments (Witjas-Paalberends et al., 2014). In contrast, our findings in primary cardiac hypertrophy show lower work output and lower energy cost of contraction with no change in mechanical efficiency in rat trabeculae. The discrepancy between our findings and those reported in patients with hypertrophic cardiomyopathy could be related to the contrasting etiologies of the two disease models. Familial hypertrophic cardiomyopathy is most commonly linked with single-point sarcomeric mutations. In contrast, the rat model used in the present study is characterized by polygenic disruption causing cardiomyocyte early terminal differentiation and compensatory hypertrophy (Porrello et al., 2009a; Prestes et al., 2018). In addition, direct comparison of in vitro tissue efficiency and in vivo whole-heart efficiency requires careful consideration. In our in vitro experiments, the quantification of mechanical efficiency

of isolated trabeculae excludes basal heat production, whereas in human in vivo studies, myocardial efficiency unavoidably includes basal oxygen consumption. In human studies, measurements are necessarily constrained to a single afterload, whereas in the present study using rodent trabeculae, measurements are performed across the complete spectrum of afterloads, thus providing a more comprehensive analysis of mechano-energetic performance.

### Limitations and future directions

The present study provides a comprehensive assessment of cardiac muscle mechanics and energetics in a rat model of primary cardiac hypertrophy. Lower activation heat observed in the hypertrophy group suggests that  $\text{Ca}^{2+}$  handling is impaired, and direct measurement of  $\text{Ca}^{2+}$  transients in future studies may be useful to further characterize the impact of primary cardiac hypertrophy on  $\text{Ca}^{2+}$  handling. Additionally, future analysis of myofilament sensitivity to  $\text{Ca}^{2+}$  and maximal  $\text{Ca}^{2+}$ -activated inotropic reserve would be informative to further understand the findings of preserved cross-bridge efficiency and economy. Finally, isometric and work-loop contraction protocols in this study employed precise control of muscle length, rather than sarcomere length. Evaluating and controlling sarcomere length in future studies may reveal effects of hypertrophy on sarcomeric contractile inhomogeneity and internal shortening.

### Conclusion

In conclusion, primary cardiac hypertrophy is associated with preserved mechanical efficiency and cross-bridge efficiency despite impairment in contractile function in isolated rat trabeculae. Impaired mechanical performance is associated with lower energy expenditure related to cardiac activation, suggesting a role for disturbances in  $\text{Ca}^{2+}$  cycling. Limitations in ATP supply may also be involved. These findings contrast with those observed in hypertensive settings, suggesting that the mechano-energetic outcomes observed in hypertensive cardiac hypertrophy may be related to the influence of increased hemodynamic load, rather than pathological heart growth per se.

### Data availability

The data that support the findings of this study are available from the corresponding author upon reasonable request.

### Acknowledgments

Henk L. Granzier served as editor.

Technical assistance in maintaining the Work-Loop Calorimeter from Dr Callum M. Zgierski-Johnston is gratefully acknowledged.

The study was supported by the Heart Foundation of New Zealand (Project Grant #1561 to K.M. Mellor; and Research Fellowship #1611 to J.-C. Han), the Health Research Council of New Zealand (Emerging Researcher First Grant #16/510 to J.-C. Han; and Sir Charles Hercus Health Research Fellowship #20/011 to J.-C. Han), and the Royal Society of New Zealand (Rutherford Foundation Fellowship #RFT-UOA1203-PD to K.M. Mellor; Fast-Start Grants #UOA1504 to J.-C. Han and #UOA1703 to K.T.; and

James Cook Research Fellowship #UOA19-UOA-012 to A.J. Taberner).

The authors declare no competing financial interests.

Author contributions: All authors contributed to the conception and design of the work; acquisition, analysis and interpretation of data; and drafting the work. All authors approved the final version of the manuscript and agreed to be accountable for all aspects of the work in ensuring that questions related to the accuracy or integrity of any part of the work are appropriately investigated and resolved. All persons designated as authors qualify for authorship, while all those who qualify for authorship are listed. All experimental work was performed at the Auckland Bioengineering Institute and the School of Medical Sciences, University of Auckland, Auckland, New Zealand.

Submitted: 3 December 2020

Accepted: 15 June 2021

### References

- Akinboboye, O.O., R.-L. Chou, and S.R. Bergmann. 2004. Myocardial blood flow and efficiency in concentric and eccentric left ventricular hypertrophy. *Am. J. Hypertens.* 17:433–438. <https://doi.org/10.1016/j.amjhyper.2004.02.006>
- Antunes, M.O., and T.L. Scudeler. 2020. Hypertrophic cardiomyopathy. *Int. J. Cardiol. Heart Vasc.* 27:100503. <https://doi.org/10.1016/j.ijcha.2020.100503>
- Bers, D.M. 2002. Cardiac excitation-contraction coupling. *Nature.* 415:198–205. <https://doi.org/10.1038/415198a>
- Cappelli, V., R. Bottinelli, C. Poggesi, R. Moggi, and C. Reggiani. 1989. Shortening velocity and myosin and myofibrillar ATPase activity related to myosin isoenzyme composition during postnatal development in rat myocardium. *Circ. Res.* 65:446–457. <https://doi.org/10.1161/01.RES.65.2.446>
- Cruickshank, J.M. 1992. Reversibility of left ventricular hypertrophy. *Blood Press. Suppl.* 1:32–33, discussion: 33–34.
- Cruickshank, J.M., J. Lewis, V. Moore, and C. Dodd. 1992. Reversibility of left ventricular hypertrophy by differing types of antihypertensive therapy. *J. Hum. Hypertens.* 6:85–90.
- de Tombe, P.P., and H.E. ter Keurs. 1991. Sarcomere dynamics in cat cardiac trabeculae. *Circ. Res.* 68:588–596. <https://doi.org/10.1161/01.RES.68.2.588>
- Feldman, H.A. 1988. Families of lines: random effects in linear regression analysis. *J Appl Physiol* (1985). 64:1721–1732. <https://doi.org/10.1152/jappl.1988.64.4.1721>
- Fitzsimons, D.P., J.R. Patel, and R.L. Moss. 1998. Role of myosin heavy chain composition in kinetics of force development and relaxation in rat myocardium. *J. Physiol.* 513:171–183. <https://doi.org/10.1111/j.1469-7793.1998.171by.x>
- Gibbs, C.L., D.S. Loiselle, and I.R. Wendt. 1988. Activation heat in rabbit cardiac muscle. *J. Physiol.* 395:115–130. <https://doi.org/10.1113/jphysiol.1988.sp016911>
- Güçlü, A., P. Knaapen, H.J. Harms, R.Y. Parbhudayal, M. Michels, A.A. Lammertsma, A.C. van Rossum, T. Germans, and J. van der Velden. 2017. Disease Stage-Dependent Changes in Cardiac Contractile Performance and Oxygen Utilization Underlie Reduced Myocardial Efficiency in Human Inherited Hypertrophic Cardiomyopathy. *Circ. Cardiovasc. Imaging.* 10:e005604. <https://doi.org/10.1161/01.RES.68.2.588>
- Han, J.-C., A.J. Taberner, P.M.F. Nielsen, R.S. Kirton, M.-L. Ward, and D.S. Loiselle. 2010. Energetics of stress production in isolated cardiac trabeculae from the rat. *Am. J. Physiol. Heart Circ. Physiol.* 299: H1382–H1394. <https://doi.org/10.1152/ajpheart.00454.2010>
- Han, J.-C., K. Tran, C.M. Johnston, P.M.F. Nielsen, C.J. Barrett, A.J. Taberner, and D.S. Loiselle. 2014. Reduced mechanical efficiency in left-ventricular trabeculae of the spontaneously hypertensive rat. *Physiol. Rep.* 2:e12211. <https://doi.org/10.14814/phy2.12211>
- Harrap, S.B., V.R. Danes, J.A. Ellis, C.D. Griffiths, E.F. Jones, and L.M.D. Delbridge. 2002. The hypertrophic heart rat: a new normotensive



- model of genetic cardiac and cardiomyocyte hypertrophy. *Physiol. Genomics*. 9:43–48. <https://doi.org/10.1152/physiolgenomics.00006.2002>
- Hickey, A.J.R., C.C. Chai, S.Y. Choong, S. de Freitas Costa, G.L. Skea, A.R.J. Phillips, and G.J.S. Cooper. 2009. Impaired ATP turnover and ADP supply depress cardiac mitochondrial respiration and elevate superoxide in nonfailing spontaneously hypertensive rat hearts. *Am. J. Physiol. Cell Physiol.* 297:C766–C774. <https://doi.org/10.1152/ajpcell.00111.2009>
- Innes, B.A., M.G. McLaughlin, M.K. Kapuscinski, H.J. Jacob, and S.B. Harrap. 1998. Independent genetic susceptibility to cardiac hypertrophy in inherited hypertension. *Hypertension*. 31:741–746. <https://doi.org/10.1161/01.HYP.31.3.741>
- Ishibashi, Y., T. Shimada, S. Nosaka, K. Sano, N. Oyake, S. Kobayashi, T. Umeno, H. Yoshitomi, and S. Morioka. 1996. Effects of heart rate on coronary circulation and external mechanical efficiency in elderly hypertensive patients with left ventricular hypertrophy. *Clin. Cardiol.* 19: 620–630. <https://doi.org/10.1002/clc.4960190808>
- Johnston, C.M., J.-C. Han, B.P. Ruddy, P.M.F. Nielsen, and A.J. Taberner. 2015. A high-resolution thermoelectric module-based calorimeter for measuring the energetics of isolated ventricular trabeculae at body temperature. *Am. J. Physiol. Heart Circ. Physiol.* 309:H318–H324. <https://doi.org/10.1152/ajpheart.00194.2015>
- Kannel, W.B. 1991. Left ventricular hypertrophy as a risk factor: the Framingham experience. *J. Hypertens. Suppl.* 9(Supplement 2):S3–S8, discussion: S8–S9. <https://doi.org/10.1097/00004872-199112002-00002>
- Kentish, J.C., H.E. ter Keurs, L. Ricciardi, J.J. Bucx, and M.I. Noble. 1986. Comparison between the sarcomere length-force relations of intact and skinned trabeculae from rat right ventricle. Influence of calcium concentrations on these relations. *Circ. Res.* 58:755–768. <https://doi.org/10.1161/01.RES.58.6.755>
- Laine, H., C. Katoh, M. Luotolahti, H. Yki-Järvinen, I. Kantola, A. Jula, T.O. Takala, U. Ruotsalainen, H. Iida, M. Haaparanta, et al. 1999. Myocardial oxygen consumption is unchanged but efficiency is reduced in patients with essential hypertension and left ventricular hypertrophy. *Circulation*. 100:2425–2430. <https://doi.org/10.1161/01.CIR.100.24.2425>
- Levy, D., R.J. Garrison, D.D. Savage, W.B. Kannel, and W.P. Castelli. 1990. Prognostic implications of echocardiographically determined left ventricular mass in the Framingham Heart Study. *N. Engl. J. Med.* 322: 1561–1566. <https://doi.org/10.1056/NEJM199005313222203>
- Livak, K.J., and T.D. Schmittgen. 2001. Analysis of relative gene expression data using real-time quantitative PCR and the 2<sup>-</sup>( $\Delta\Delta C_T$ ) Method. *Methods*. 25:402–408. <https://doi.org/10.1006/meth.2001.1262>
- Loiselle, D.S. 1987. Cardiac basal and activation metabolism. *Basic Res. Cardiol.* 82(Suppl 2):37–50. [https://doi.org/10.1007/978-3-662-11289-2\\_4](https://doi.org/10.1007/978-3-662-11289-2_4)
- Mellor, K.M., C.L. Curl, C. Chandramouli, T. Pedrazzini, I.R. Wendt, and L.M.D. Delbridge. 2014. Ageing-related cardiomyocyte functional decline is sex and angiotensin II dependent. *Age (Dordr.)*. 36:9630. <https://doi.org/10.1007/s11357-014-9630-7>
- Miyata, S., W. Minobe, M.R. Bristow, and L.A. Leinwand. 2000. Myosin heavy chain isoform expression in the failing and nonfailing human heart. *Circ. Res.* 86:386–390. <https://doi.org/10.1161/01.RES.86.4.386>
- Pham, T., K. Tran, K.M. Mellor, A. Hickey, A. Power, M.-L. Ward, A. Taberner, J.-C. Han, and D. Loiselle. 2017. Does the intercept of the heat-stress relation provide an accurate estimate of cardiac activation heat? *J. Physiol.* 595:4725–4733. <https://doi.org/10.1113/JP274174>
- Pham, T., L. Nisbet, A. Taberner, D. Loiselle, and J.-C. Han. 2018. Pulmonary arterial hypertension reduces energy efficiency of right, but not left, rat ventricular trabeculae. *J. Physiol.* 596:1153–1166. <https://doi.org/10.1113/JP275578>
- Pogwizd, S.M., K.R. Sipido, F. Verdonck, and D.M. Bers. 2003. Intracellular Na in animal models of hypertrophy and heart failure: contractile function and arrhythmogenesis. *Cardiovasc. Res.* 57:887–896. [https://doi.org/10.1016/S0008-6363\(02\)00735-6](https://doi.org/10.1016/S0008-6363(02)00735-6)
- Porrello, E.R., J.R. Bell, J.D. Schertzer, C.L. Curl, J.R. McMullen, K.M. Mellor, R.H. Ritchie, G.S. Lynch, S.B. Harrap, W.G. Thomas, and L.M.D. Delbridge. 2009a. Heritable pathologic cardiac hypertrophy in adulthood is preceded by neonatal cardiac growth restriction. *Am. J. Physiol. Regul. Integr. Comp. Physiol.* 296:R672–R680. <https://doi.org/10.1152/ajpregu.90919.2008>
- Porrello, E.R., A. D'Amore, C.L. Curl, A.M. Allen, S.B. Harrap, W.G. Thomas, and L.M.D. Delbridge. 2009b. Angiotensin II type 2 receptor antagonizes angiotensin II type 1 receptor-mediated cardiomyocyte autophagy. *Hypertension*. 53:1032–1040. <https://doi.org/10.1161/HYPERTENSIONAHA.108.128488>
- Power, A.S.C., T. Pham, D.S. Loiselle, D.H. Crossman, M.-L. Ward, and A.J. Hickey. 2016. Impaired ADP channeling to mitochondria and elevated reactive oxygen species in hypertensive hearts. *Am. J. Physiol. Heart Circ. Physiol.* 310:H1649–H1657. <https://doi.org/10.1152/ajpheart.00050.2016>
- Prestes, P.R., F.Z. Marques, G. Lopez-Campos, P. Lewandowski, L.M.D. Delbridge, F.J. Charchar, and S.B. Harrap. 2018. Involvement of human monogenic cardiomyopathy genes in experimental polygenic cardiac hypertrophy. *Physiol. Genomics*. 50:680–687. <https://doi.org/10.1152/physiolgenomics.00143.2017>
- Taberner, A.J., J.-C. Han, D.S. Loiselle, and P.M.F. Nielsen. 2011. An innovative work-loop calorimeter for in vitro measurement of the mechanics and energetics of working cardiac trabeculae. *J. Appl. Physiol.* (1985). 111: 1798–1803. <https://doi.org/10.1152/jappphysiol.00752.2011>
- ter Keurs, H.E., W.H. Rijnsburger, R. van Heuningen, and M.J. Nagelsmit. 1980. Tension development and sarcomere length in rat cardiac trabeculae. Evidence of length-dependent activation. *Circ. Res.* 46:703–714. <https://doi.org/10.1161/01.RES.46.5.703>
- Tingleff, J., M. Munch, T.J. Jakobsen, C. Torp-Pedersen, M.E. Olsen, K.H. Jensen, T. Jørgensen, and M. Kirchhoff. 1996. Prevalence of left ventricular hypertrophy in a hypertensive population. *Eur. Heart J.* 17: 143–149. <https://doi.org/10.1093/oxfordjournals.eurheartj.a014672>
- Tran, K., J.-C. Han, E.J. Crampin, A.J. Taberner, and D.S. Loiselle. 2017. Experimental and modelling evidence of shortening heat in cardiac muscle. *J. Physiol.* 595:6313–6326. <https://doi.org/10.1113/JP274680>
- Tran, K., A.J. Taberner, D.S. Loiselle, and J.-C. Han. 2020. Energetics Equivalent of the Cardiac Force-Length End-Systolic Zone: Implications for Contractility and Economy of Contraction. *Front. Physiol.* 10:1633. <https://doi.org/10.3389/fphys.2019.01633>
- Widén, C., and C.J. Barclay. 2006. ATP splitting by half the cross-bridges can explain the twitch energetics of mouse papillary muscle. *J. Physiol.* 573: 5–15. <https://doi.org/10.1113/jphysiol.2006.104992>
- Witjas-Paalberends, E.R., A. Güçlü, T. Germans, P. Knaapen, H.J. Harms, A.M.C. Vermeer, I. Christiaans, A.A.M. Wilde, C. Dos Remedios, A.A. Lammertsma, et al. 2014. Gene-specific increase in the energetic cost of contraction in hypertrophic cardiomyopathy caused by thick filament mutations. *Cardiovasc. Res.* 103:248–257. <https://doi.org/10.1093/cvr/cvu127>
- Wong, Y.Y., G. Ruiter, M. Lubberink, P.G. Raijmakers, P. Knaapen, J.T. Marcus, A. Boonstra, A.A. Lammertsma, N. Westerhof, W.J. van der Laarse, and A. Vonk-Noordegraaf. 2011. Right ventricular failure in idiopathic pulmonary arterial hypertension is associated with inefficient myocardial oxygen utilization. *Circ. Heart Fail.* 4:700–706. <https://doi.org/10.1161/CIRCHEARTFAILURE.111.962381>